Nanoscale

ROYAL SOCIETY OF CHEMISTRY

MINIREVIEW

View Article Online
View Journal | View Issue

Cite this: *Nanoscale*, 2024, **16**, 6383

Engineering strong man-made cellulosic fibers: a review of the wet spinning process based on cellulose nanofibrils

Zihuan Zhang, †[a,b] Yuying Kong, †[a,b] Junqi Gao, †[a,b] Xiao Han, [a,b] Zechun Lian,[a] Jiamin Liu,[a] Wen-Jun Wang [a,b] and Xuan Yang *[a,b]

With the goal of sustainable development, manufacturing continuous high-performance fibers based on sustainable resources is an emerging research direction. However, compared to traditional synthetic fibers, plant fibers have limited length/diameter and uncontrollable natural defects, while regenerated cellulose fibers such as viscose and Lyocell suffer from inferior mechanical properties. Wet-spun fibers based on nanocelluloses especially cellulose nanofibrils (CNFs) offer superior mechanical performance since CNFs are the fundamental high-performance building blocks of plant cell walls. This review aims to summarize the progress of making CNF wet-spun fibers, emphasizing on the whole wet spinning process including spinning suspension preparation, spinning, coagulation, washing, drying and post-stretching steps. By establishing the relationships between the nano-scale assembling structure and the macroscopic changes in the CNF dope from gels to dried fibers, effective methods and strategies to improve the mechanical properties of the final fibers are analyzed and proposed. Based on this, the opportunities and challenges for potential industrial-scale production are discussed.

Received 30th November 2023,
Accepted 21st February 2024

DOI: 10.1039/d3nr06126d

rsc.li/nanoscale

Introduction

Fiber materials have accompanied and promoted the evolution of human civilization, from cloth, paper, and packaging in daily life to cables, fillers and hoses in industry. Their unique 1-D feature gives them broad flexibility in structural design and they can be manufactured into more complex shapes and architecture.

With the development of the polymer industry, one corresponding product, synthetic fibers, has been dominating many

[a]*Key Laboratory of Biomass Chemical Engineering of Ministry of Education, State Key Laboratory of Chemical Engineering, College of Chemical and Biological Engineering, Zhejiang University, Hangzhou 310027, P.R. China. E-mail: xuan.yang@zju.edu.cn*
[b]*Institute of Zhejiang University-Quzhou, Quzhou, 324000, P.R. China*
† These authors contributed equally to this work.

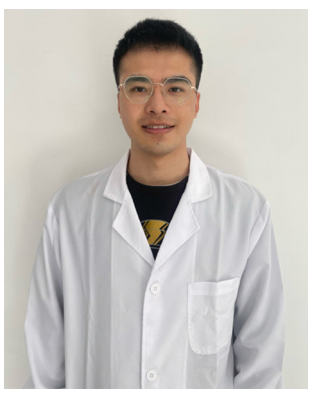

Zihuan Zhang

Zihuan Zhang received his B.E. degree in Chemical Engineering and Technology from Zhejiang University in 2022. He is continuing as a Ph.D. candidate under the supervision of Prof. Xuan Yang. His research mainly focuses on advanced structural and functional materials design based on nanocellulose.

Yuying Kong

Yuying Kong is currently a Ph.D. candidate in Chemical Engineering and Technology at Zhejiang University under the supervision of Prof. Xuan Yang. Her current research interest focuses on nanocellulose-based functional materials, especially for sensing applications.

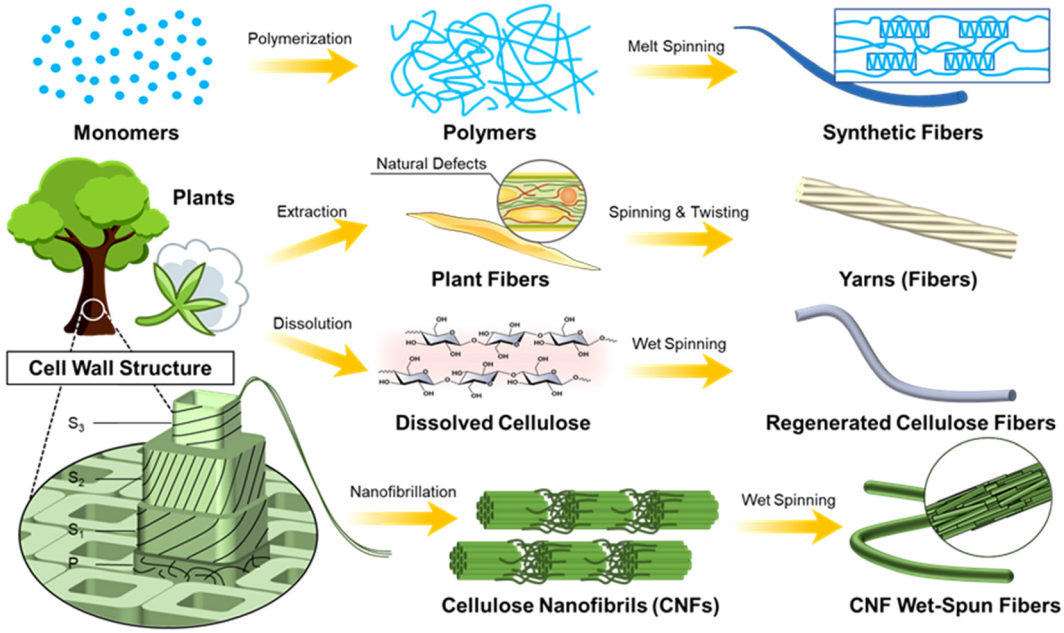

Fig. 1 Synthesis routes to different types of man-made fibers.

application areas, with a global market size valued at USD 66.11 billion in 2022.[1] Compared to conventional natural plant fibers, they have preferred mechanical performance and high production rate with cheaper price, as well as easy to tune surface properties.[2] One of the reasons for such superior properties is their production route: polymerization and melt spinning. Controlled polymerization can give a preferred chain structure, so that the basic chemical and physical properties can be tailored precisely, while the melt processing ability (related to rheology performance) can be tuned to benefit the spinning process, inducing favorable chain alignment and crystallization (Fig. 1).[3,4]

As an alternative choice, plant fibers actually have been used for thousands of years, such as garments, paper, and tools.[5] Compared to synthetic fibers which are produced using a bottom–up assembling process all the way from the molecular level, the production of plant fibers follows a top–down approach, in which they are extracted or liberated from plant tissues. Viewing it from a composite perspective, one single plant fiber is made from cellulose nanofibrils (CNFs) as reinforcing fillers embedded in the hemicellulose and lignin matrix.[6–10] Importantly, building blocks in the plants, fibers, have evolved to the best extent. They synthesize glucose units from C, H, and O atoms and polymerize them into cellulose

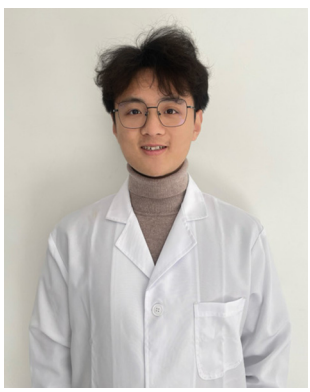

Junqi Gao

Junqi Gao received his B.E. degree in Chemical Engineering and Technology from Zhejiang University, China in 2023. He is pursuing his Ph.D. at Zhejiang University under the guidance of Prof. Xuan Yang. His current research focuses on the optimization of the nanocellulose wet spinning process.

Xuan Yang

Dr Xuan Yang is a tenure-track "100-talent" professor at the College of Chemical and Biological Engineering, Zhejiang University. He received his M.A. Sc. and Ph.D. degrees at McMaster University, Canada (supervisor: Prof. Emily Cranston) and KTH Royal Institute of Technology, Sweden (supervisor: Prof. Lars Berglund), respectively. Xuan's research group is currently focusing on biomass chemical engineering, especially with a scope of "by taking inspiration from nature and harnessing bio-based components, we can engineer high-performance materials to meet the growing demand for sustainable products and processes".

molecules, which are then aligned and packed into crystalline fibrils using favorable hydrogen bonding and van der Waals forces.[11,12] These CNFs have superior mechanical properties (a Young's modulus of 65–130 GPa,[13,14] and a strength of 1–3 GPa[15]), as well as a high aspect ratio (a width of ~4 nm and a length up to a few μm), making them superior back-bone fillers to provide mechanical strength to the plant fibers. Moreover, they are constructed into different layers (primary and secondary 1-2-3) to form the fiber cell walls (Fig. 1).[16]

The most critical issue or drawback of plant fibers for loading applications is natural defects including a limited length/diameter, a hollow structure, and uncontrollable individual differences. Nevertheless, the process of extracting plant fibers is also challenging which may introduce damage during the chemical and physical processes.[17,18] For example, the chemical pulping process intends to liberate wood fibers by mainly removing the lignin-rich middle lamellae without causing direct physical damage to the fibers.[19] However, the unwanted degradation of cellulose and hemicellulose actually alters the fiber cell wall structure on the molecular- and nanoscale.[20]

To overcome these disadvantages of natural fibers, regenerated cellulose fibers such as viscose and Lyocell are developed. It involves the complete dissolution of cellulose polymer chains, followed by a regeneration process to repack these chains into macro-size fibers. Such a process is termed wet spinning.[21] The use of dissolved cellulose polymers greatly boosts the processing ability to control the final fiber structure and enable continuous production. However, such a process is based on damaging the original crystalline cellulose structure, resulting in relatively weaker mechanical properties (a modulus of 11–16 GPa, a strength of 486–593 MPa),[22,23] compared to many synthetic fibers. And yes, they have much inferior mechanical properties compared to their original sources – plant fibers. Moreover, harsh solvents are needed to dissolve cellulose (NaOH and CS_2 for viscose and NMMO hydrate for Lyocell) which causes environmental concerns.[24]

Under the scheme of making man-made fibers using sustainable resources, CNFs have become an emerging building block.[25,26] As discussed before, CNFs are the structural fundamental building blocks of plant fibers. With the development of nanotechnology, CNFs can be obtained based on different plants through a series of pretreatments and nanofibrillation processes.[27–29] This leads to various widths/lengths, yet the majority have a width <10 nm and a length >500 nm (Fig. 2)[26,30–33] and residual surface components including hemicellulose and lignin. Among them, CNFs prepared using 2,2,6,6-tetramethylpiperidine-1-oxyl radical (TEMPO)-mediated oxidation have been the most classical method, which generates carboxyl groups at the C-6 position to give high colloidal stability.[34,35] Moreover, CNFs belong to the family of nanocelluloses, which contains two other members: cellulose nanocrystals (CNCs) and bacterial celluloses (BCs). The most distinct difference is the dimension/morphology. Compared to CNFs, CNCs and BCs have a large width of >5 nm, while CNCs have a short length (normally <200 nm) and BCs have a much longer length (Fig. 2).[36–39]

Nanocelluloses, CNFs in most cases, have been explored to produce long fibers with a diameter in microns using the wet spinning process.[40] Note that the final fibers are also termed filaments in the literature. Here, we choose to name them CNF fibers to easily differentiate them from synthetic fibers, natural fibers and regenerated fibers. Such a CNF fiber can be seen as a long bundle of CNFs with a preferred assembling structure, which utilizes the advantages of CNFs' high aspect ratio and high mechanical properties. From the CNF aspect, CNFs have unique features crossing both semi-crystalline polymeric materials and colloidal particles, resulting in a superior assem-

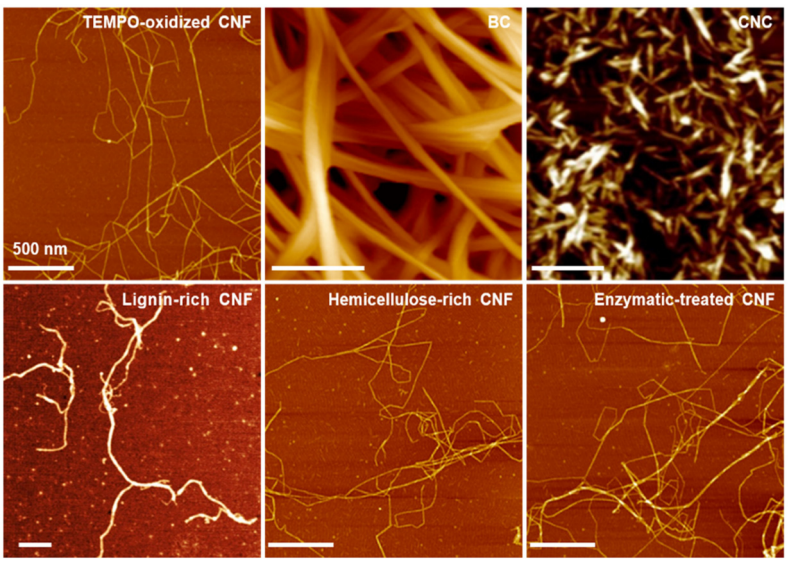

Fig. 2 AFM images of different types of nanocelluloses. Adapted with permission from ref. 122 and 123. Copyright 2021, 2019 Springer Nature.[82,122–124]

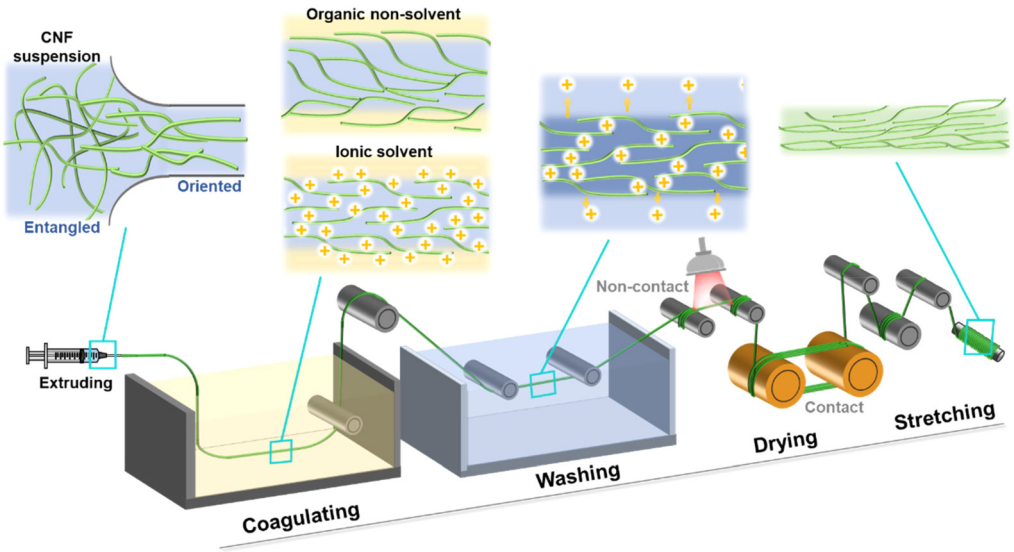

Fig. 3 Schematic of the continuous wet spinning process and the nanostructure changes from CNF suspensions to dried fibers.

bling ability.[6,26] Promisingly, such CNF wet-spun fibers have superior mechanical properties (tensile strength and Young's modulus of up to 650 MPa and 40 GPa, respectively), compared to regenerated cellulose fibers, natural fibers and even many synthetic fibers. Thus, CNFs have great potential to be used as reinforcing fillers and special textiles and may even pave new application areas where conventional fiber materials are incompetent.

In this review, we aim to first emphasize the wet spinning process to prepare CNFs, including spinning suspension preparation, the spinning/extruding step, coagulation, drying and stretching (Fig. 3). From the nanostructure aspect, the CNF networks experience a series of changes including randomly distributed, deformed and oriented, crosslinked/compressed, densified, and further aligned confirmations (Fig. 3). The main purpose is to establish a deep understanding of the relationships between the nano-scale assembling structure and the macroscopic changes in the CNF dope from gels to dried fibers. Moreover, the mechanical properties of the final CNF fibers are selected as the main evaluating factor. Finally, the industrial production perspective is analyzed.

Preparation of CNF spinning suspensions

The first step of the wet spinning process is to prepare the CNF spinning suspensions, which normally behave as a viscous gel. Upon spinning, such a gel suspension is deformed into a spinning flow by external forces (*i.e.*, shear force), which corresponds to the assembling structure of nanocellulose fibrils from isotropic to oriented state at the nanoscale (Fig. 4a). The ideal case is to orientate the CNFs as much as possible without causing the discontinuity of the extruded gels. In other words, it is to balance the deformation ability and the fibril connectivity of the CNF networks within the spinning gels, which are essentially correlated to the viscoelastic properties. Although it is hard to characterize such dynamic structural changes of each CNF during the wet spinning process, the rheological properties of the prepared gel suspensions can be characterized easily, which can be used to study the nano-structural changes and even predict the spinnability of certain CNF spinning suspensions.

With high colloidal stability and high aspect ratio, CNFs under aqueous conditions (suspension) share many attributes close to dissolved polymers.[40] Consequently, at low concentrations, CNF suspensions also exhibit a typical shear thinning behavior (decreasing viscosity against increasing shear rate).[41] Typically, the apparent shear viscosity measured in a steady shear flow (η), as well as the dynamic modulus (storage modulus G' and loss modulus G'') measured from the small amplitude oscillatory shear (SAOS) test are characterized, which reflect the viscoelastic properties of the nanocellulose fibril network.[41] Examples of apparent shear viscosity and dynamic modulus measurements for TEMPO-CNF suspensions at various concentrations are shown in Fig. 4b and c.

The measured apparent shear viscosity can be fitted with the Ostwald-de Waele power law:[42,43]

$$\eta = K\dot{\gamma}^{n-1} \quad (1)$$

where η is the apparent shear viscosity, $\dot{\gamma}$ is the shear rate, and K and n are the consistency and flow behavior indices, respectively. K and n reflect the fibrillar crowding conditions and shear thinning degree, respectively.

Importantly, both K and G' have a positive linear correlation with c^x, where c is the CNF concentration.[44] This is in agreement with most studies that optimized the rheological behavior of CNF spinning suspensions by changing the concentrations. However, the reported values of the power law exponent x have a large range (2–5),[45–47] indicating the contri-

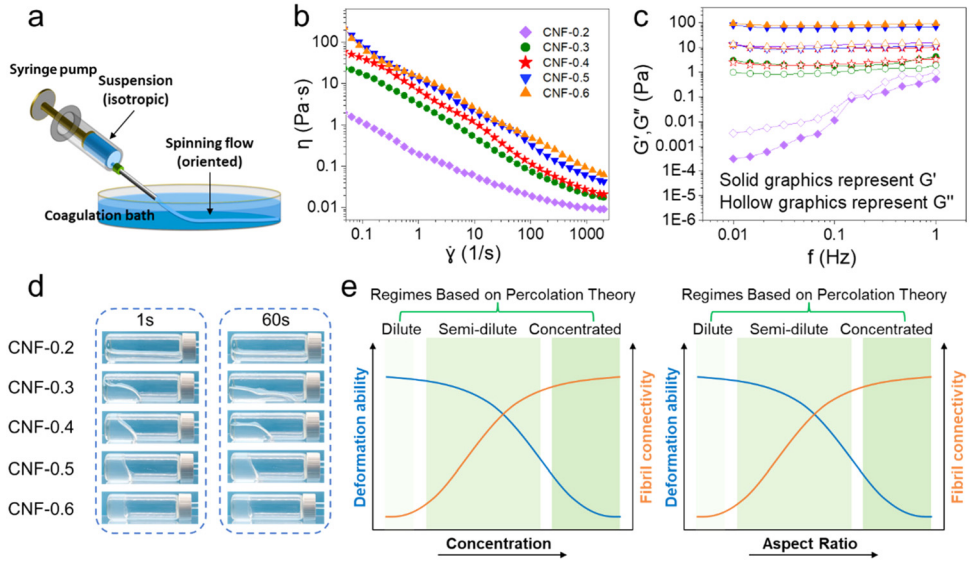

Fig. 4 (a) Schematic of CNF extrusion using a syringe pump.[53] Adapted and modified with permission from ref. 53. Copyright 2014 ACS. Rheological behavior of TEMPO-CNF suspensions at different concentrations: (b) apparent shear viscosity as a function of shear rate, (c) storage and loss modulus as a function of oscillatory frequency and (d) virtual flowability.[51] Adapted with permission from ref. 51. Copyright 2023 Elsevier. (e) Estimated trends in the deformation ability and fibril connectivity for CNF suspensions with increasing concentrations and aspect ratios.

butions from other contributing factors are affecting the rheological behavior of CNF suspensions.

As the rheological properties of CNF suspensions can be treated as a network with rod-like particles, percolation theory can be applied. Based on the volumetric concentration ($\varnothing$) and geometrical aspect (A) of CNF, CNF suspensions can be roughly divided into three regimes:[48]

(1) Dilute regime ($\varnothing < A^{-2}$), where each fibril has almost no chance to be in contact with each other, and is allowed to freely rotate in three dimensions, thus leading to a liquid-like ($G' \ll G''$) and Newtonian behavior (constant viscosity against changing shear rate). Note that suspensions in this regime are unsuitable for spinning as there is no connectivity to support the fiber structure.

(2) Semi-dilute regime ($A^{-2} < \varnothing < A^{-1}$), where there are increasing contacts and flocculation between fibrils, partially limiting their mobility. In particular, a gel transition point usually falls within this regime, as nanocellulose suspensions change from the Newtonian fluidic state to the viscoelastic state, which in rheological terms, reflects on the slope change in viscosity–concentration linear curve and the cross-over at which G' surpasses G''. Suspensions become increasingly gel-like in this regime, nevertheless they can still be considered in the flowing state as a stable gel is formed when G' is at least one order of magnitude higher than G''.[49]

(3) Concentrated regime ($\varnothing > A^{-1}$), where multiple contacts between fibrils lead to an interconnected network with minimal fibril mobility, thus giving rise to increasingly gel- or solid-like behavior ($G' \gg G''$). In particular, when $\varnothing > 1.5A^{-1}$, suspensions evolve into a volume-spanning arrested state (VAS), where each fibril is tightly "locked" in the network and suspensions are non-flowing.[50]

To give a visual impression, the CNF suspension flow behavior at different concentrations is shown in Fig. 4d, where CNF-0.2, -0.3, and -0.4 are in the flowing state, as in the semi-dilute regime, CNF-0.5 and -0.6 are in the non-flowing state, as in the concentrated regime.[51] Furthermore, the spinnability of CNF suspensions is balancing between the deformation ability and fibril connectivity, which links to the CNF concentration and aspect ratio (Fig. 4e). Instead of characterizing and evaluating the rheological behavior in depth, or calculating based on the percolation theory, most studies have relied on empirical values, for instance, using a CNF suspension with concentration above 1 wt%,[42,52,53] or requiring an apparent shear viscosity on the order of 1 Pas at the shear rate applied in spinnerets.[52] Moreover, it is well known that CNF surface charges and processing history also influence the rheological behavior heavily, yet these have rarely been investigated.

Connecting CNF parameters to fiber properties in wet spinning is important for fiber quality optimization, while elucidating the correlations by simply comparing each parameter from different reported works is difficult and probably fruitless, as it requires precise variable control for CNF attributes and spinning conditions, which is impractical.[55] Here, we aim to discuss the effects of concentration, aspect ratio, surface charge and processing history in a comprehensive way, particularly using rheology and percolation theory as useful tools to emphasize the properties of CNF spinning suspensions.

Concentration of CNF suspensions

As a quick and easy controlling parameter, the concentration of CNF suspensions has been the first choice to alter the viscosity which links to spinnability. With a large attempting range (1 to 10 wt%) based on unmodified CNFs, suspensions

with a relatively medium concentration (2 wt%) were discovered to produce fibers with the highest orientation, leading to superior mechanical properties (Fig. 5a).[52] These results were explained by the following mechanism: (1) low concentration (viscosity) favors flow-induced alignment during shear flow or extensional flow, while the reduced interfibrillar interaction (too low concentration) cannot support a rigid network or even make CNFs dilute to "nothing" in the coagulation bath; (2) high concentration (viscosity) means a high density of interfibrillar interaction, which disturbs flow-induced alignment,[52] or in extreme situations, the CNFs in suspensions cannot be broken up into the shear thinning state or possess a significant degree of local fibril aggregation that remains in the spun fibers.[56]

However, the fact that CNFs of different types vary drastically in rheological properties/interfibrillar interactions makes it impossible to draw one suitable concentration range that suits all. Here, using the regime classification mentioned above instead of specific concentration values, it is found that studies have generally used CNF suspensions in the concentrated regime, normally when CNFs form a strong gel network ($G' \gg G''$), in order to sustain a stable fiber structure. For example, unmodified CNFs (≥2 wt%),[57–60] TEMPO-CNFs (≥1 wt%),[53,61] and BCs (≥1.8 wt%)[62–64] have been used for wet spinning and essentially demonstrated higher orientation at decreased concentrations (viscosity).

For negatively charged CNFs containing carboxyl groups, it has been reported that suspensions in a semi-dilute regime can also be used for fiber spinning, and can yield fibers with even higher orientation and mechanical performance compared to those in the concentrated regime.[56] Though suspensions in the semi-dilute regime are usually used in microfluidic spinning,[65–67] one study has shown that wet-spun fibers produced from carboxymethylated CNFs in the semi-dilute regime (0.3 wt%, $G' \approx G''$) possess higher orientation and mechanical properties than those in the concentrated regime (1.2 wt%, $G' \gg G''$) (Fig. 5b and c).[56]

More recently, a new standard measured by the creep recovery (CR) test was reported, in which it was discovered that TEMPO-CNFs with a charge density of 820 μmol g^{-1} form an increasingly elastic network with a decreasing deformation ability above the gel point concentration ($G' \approx G''$),[51] which links to the cross-point of the curves in Fig. 4e. The predicted optimal concentration is between 0.3 and 0.4 wt%.[51] The lowest concentration to form a gel after coagulation is tested to be 0.3 wt%, although it cannot maintain its regular shape due to the delayed gelation time upon coagulation (Fig. 5e). In comparison, 0.4 wt% balanced the spinnability and preferred fiber orientation (Fig. 5f). Similarly, carboxymethylated CNFs (degree of substitution of 0.1) with $G' \approx G''$ were successfully spun into fibers using HCl as the coagulation bath.[56]

Aspect ratio of CNFs

For polymers used in melt spinning or wet spinning, molecular weight is a critical parameter of the starting materials. For CNFs as spinning materials, their dimension, especially the aspect ratio is equally important.

It is well known that the aspect ratio of CNFs depends on the sources and preparation processes (chemical pretreatment and mechanical fibrillation). Generally speaking, CNFs based on tunicates have much higher aspect ratios (>500) than the ones sourced from woods (<200), and therefore lead to higher hydrogel viscosity.[55] Consequently, Iwamoto *et al.* reported that fibers spun from tunicate CNFs have much lower orientation indexes compared to those based on wood CNFs (0.44–0.54 compared to 0.65–0.72), using a similar wet spinning process (Fig. 5g).[59] Although CNFs with high aspect ratios should be able to form more entanglements, it also drives up the difficulty of being aligned along shear forces. Moreover, CNFs with too high aspect ratios (*i.e.*, BCs) tend to form a locked system starting from a very low concentration, leading to high porosity in the final fibers to harm mechanical properties, which is not preferred (Fig. 5h).[63]

Other than having a high threshold, the aspect ratio of CNFs should also have a low threshold to ensure the connectivity of fibrils maintaining a continuous network. For example, cellulose nanocrystals (CNCs, a type of nanocellulose with a much lower aspect, normally <50) have also been used to obtain wet-spun fibers, yet need to be mixed with other polymers like alginate[68] or dissolved cellulose[69] to allow continuous spinning. Although microfluidic spinning based on acid-induced gelation has realized spinning from pure CNC suspensions, the mechanical properties of the obtained fibers are far from optimal, probably due to the lack of fibril entanglement in the fiber structure.[70,71] Moreover, microfluidic equipment is still under development for industrial scale production.

One more interesting thing we want to do here is to predict a suitable concentration for wet spinning based on percolation theory. According to our previous discussion, CNF suspensions should be in the semi-dilute regime ($A^{-2} < \varnothing < A^{-1}$). Using CNFs with a typical aspect ratio of ~200 (a diameter of 5 nm and a length of 1 μm), the preferred CNF concentration is predicted to be 0.004–0.75 wt%. Furthermore, in the optimized $G' \approx G''$ state in which the deformation ability and fibril connectivity are balanced, if each fibril has at least 3 contact points to form a connected rigid network ($\phi = 90A^{-2}$),[72] then the optimal concentration is predicted to be ~0.34 wt%. This is in very good agreement with the study using TEMPO-CNFs with an aspect ratio of ~200.[51]

Surface charge of CNFs

Beyond the concentration and aspect ratio, the surface charge of CNFs is also very important for these colloidal suspensions. CNFs without any surface charge have inferior colloidal stability, which is not suitable for the wet spinning process due to unwanted aggregation and low viscosity. Thus, most studies used TEMPO-CNFs with high surface charges. The effects of charge on CNF rheological properties are multifaceted. For TEMPO-CNFs, with increasing charge density (380–1360 μmol g^{-1}), the viscosity first increases and then decreases (Fig. 5i).[72] The increase is attributed to the elevated fibrillation level by induced electrostatic repulsion, leading to a higher aspect

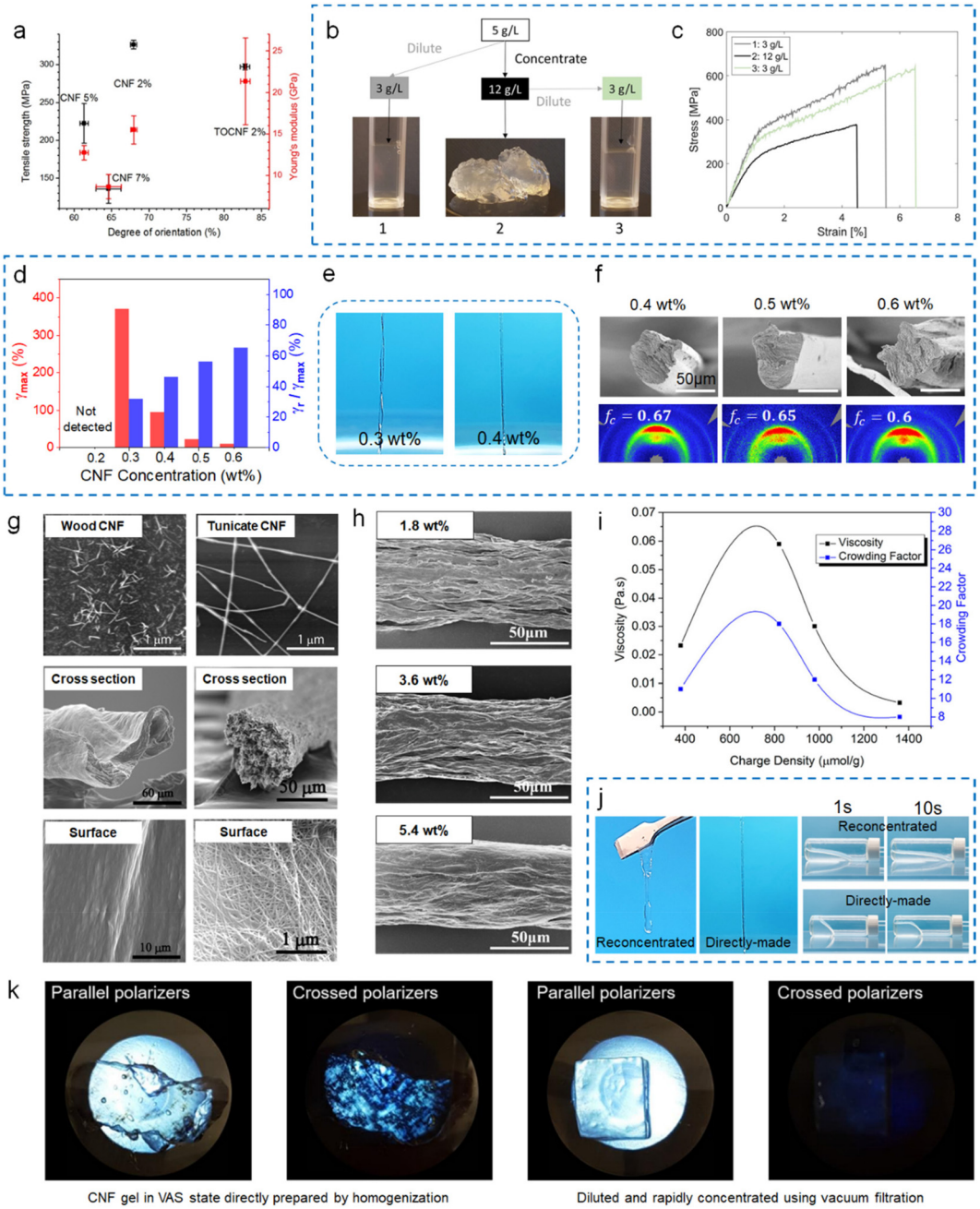

Fig. 5 (a) Fiber tensile strength and Young's modulus as a function of the degree of orientation, and error bars correspond to the standard deviation.[52] (b) Images of the three starting suspensions and a schematic of the dilution and concentration routes.[56] (c) Representative stress–strain curves for fibers produced from the three samples.[56] (d) Maximum deformation (γ_{max}) and recovery deformation rate (γ_r/γ_{max}) of the CNF suspension with different concentrations.[51] (e) Photos of still-wet fibers spun from 0.3 wt% and 0.4 wt% concentrations.[51] (f) SEM image of the cross-section and degree of orientation of different CNF fibers.[51] (g) TEM images of CNFs extracted from wood and tunicate and SEM images of their corresponding spun fibers showing cross-section and surface.[59] (h) SEM images showing the surface of fibers spun from TEMPO-oxidized BC with different concentrations.[63] (i) Steady shear viscosity at 0.1 s^{-1} and crowding factor of 0.05 wt% CNF suspensions as a function of charge density.[72] (j) Photos and virtually flowability of reconcentrated and directly-made 0.4 wt% CNF suspensions.[51] (k) Birefringence (crossed polarizers) of CNF gels showing local domains of fibril alignment: (left panel) directly prepared by homogenization and (right panel) diluted and rapidly concentrated back.[54] (a) Adapted with permission from ref. 52. Copyright 2016 Springer Nature. (d–f and j) Adapted with permission from ref. 51. Copyright 2023 Elsevier. (g) Adapted with permission from ref. 59. Copyright 2011 ACS. (h) Adapted with permission from ref. 63. Copyright 2017 ACS. (k) Adapted with permission from ref. 54. Copyright 2019 ACS.

ratio and narrower size distribution, giving rise to a stronger network structure; the decrease is due to (1) the increased osmotic repulsion force between CNFs, leading to lower agglomeration propensity and (2) reduced fibril length (aspect ratio) as a result of excessive chemical modification, leading to a lower fibril crowding degree.[72]

Besides, charge density directly influences the flow-to-nonflow transition behavior of CNF suspensions. In the case of CNFs with low surface charges (*i.e.*, unmodified CNFs or BCs), their weak electrostatic repulsion may be overcome by attractive van der Waals interactions at increasing concentrations, giving rise to aggregation and earlier formation of a non-flowing VAS state.[50] The case is more complicated for CNFs with sufficiently high surface charges. Screening electrostatic repulsion by increasing ionic strength (adding salts) or adjusting pH can lead to VAS formation, while the exception is when the counterion concentration is too low to disturb colloidal stability, only to increase the VAS threshold instead because of the reduced double layer thickness and effective volume fraction.[50,73,74] Notably, unlike VAS systems dominated by repulsive forces (termed glasses) realized by mobility constraints at high concentrations, VAS systems dominated by attractive forces (termed gels) can resist re-dispersion by dilution.[50]

Understanding surface charge as a factor for the gelation mechanism of CNF systems is vital as it also concerns an integral part of the wet spinning process (*i.e.*, coagulation). CNFs with high surface charges tend to have high affinity to water molecules due to the hydration effect, which prolongs the time in the following coagulation and drying processes. Moreover, when using HCl or $CaCl_2$ as the coagulation bath, the surface charge of CNFs will affect the diffusion efficiency of ions into the CNF network. For instance, for CNFs with low surface charge, coagulation will not be sufficient. In other words, the intensity of the transition from a flow state to the gel state with the introduction of crosslinks is affected by the surface charge density of CNFs.[50,75,76] While for CNFs with high surface charge, coagulation by organic non-solvents will not be suitable as the interfibrillar repulsion is too high to be overcome by simple solvent exchange.[77]

Processing history of CNF suspensions

The distribution state of CNFs within the spinning suspension is very important, which can be reflected in the rheological behavior. The processing history such as long time storage, concentration, or re-dilution will affect this. In most cases, CNFs are disintegrated from pulps using high-pressure homogenization, and the starting concentration should be neither too low, which leads to inferior shearing/tearing on the pulps, nor too high, which causes clogging issues.[59,78,79] As discussed before, the CNF concentration should be sufficiently high for optimized wet spinning, and the as-prepared CNF suspensions cannot be directly used. For the case of having too low concentration, an up-concentration process is generally performed by vigorous stirring or rotating under heating conditions (introducing vacuum in some cases) to evaporate water. However, it is demonstrated that constant stirring and heating may cause local fibril alignment or aggregations,[54,80] reflected in a more viscous response in rheological behavior.[51] This suggests a less stable structure of the fibril system in suspensions, thus leading to worse spinnability (Fig. 5j). Note that up-concentration can also be done by centrifugation or ultra-filtration, but both are energy extensive which will be discussed later. In the current state-of-the-art regime, disintegration of pulps has also been done at concentrations as high as 1–2 wt%. However, this is well above the VAS threshold for common CNFs, which yields an inhomogeneous network, unless subsequent dilution is performed (Fig. 5k).[54,80] In contrast, CNF suspensions prepared by direct fibrillation in a kitchen blender, accompanied by gradual dilution, showed excellent homogeneity and spinnability.[51] It is expected that in industrial practice, large quantities of CNF suspensions may be stored for a long time, and the concentrating process seems inevitable. How to ensure a uniform dispersion state of fibrils in a bulk suspension remains a both scientific and engineering question.

Chemical composition of CNFs

The selective disintegration of lignocellulosic materials renders CNFs with alterable residual native components (*i.e.*, hemicellulose and lignin) and surface chemistry, which opens up a new avenue for high-performance wet-spun fiber processing with tailored properties. However, most relevant studies focus on the use of TEMPO-CNFs or carboxymethylated CNFs which predominantly contain cellulose. Here, we attempt to emphasize the wet spinning potential of hemicellulose-rich or lignin-rich CNFs. And we do believe new types of CNFs will broaden our research scope of wet-spun CNF fibers.

For hemicellulose-rich CNFs (also termed holo-CNFs), they enjoy good colloidal stability due to (1) charged groups within the hemicellulose layer and (2) steric hindrance by the hygroscopic hemicellulose layer swollen in water,[81] which is a favourable property for wet spinning. Moreover, their well-preserved crystalline structure and ultra-long fibril morphology are expected to optimize the mechanical properties of ensuing cellulosic materials.[82,83] However, the drawback is their low viscosity due to a low fibrillar crowding degree and especially the inhibited coalescence of fibrils by hemicellulose during coagulation, leading to inferior wet strength. Therefore, high concentration suspensions or special designs of the coagulation process are supposed to address this issue.[84]

For lignin-rich CNFs (also termed L-CNFs), the utilization of lignin is expected to increase the utilization of lignocellulosic materials and endow fibers with unique functionalities including hydrophobicity, UV shielding and antioxidation.[83] However, residual lignin significantly disturbs the nanofibrillation efficiency, thus they usually exhibit thick and non-uniform morphologies in most literature reports,[85] unless chemical pretreatments are performed to introduce charge repulsion before mechanical fibrillation. Consequently, the large fibril bundles, poor fibril binding capacity, and remaining lignin agglomerates impair the spinnability, disturb fibril alignment and even result in high roughness of the fiber surface.[84,86]

Spinning parameters

After the CNF spinning suspensions are prepared, they are extruded into a spinning flow to initiate the wet spinning process. The spinning scheme, in other words, the equipment design determines how the spinning flow or the coagulation process is applied. Regarding the controllable parameters, the spinning rate has been the key one which can be easily tuned and can be interpreted based on already established theory.

Spinning schemes

The most common spinning scheme for CNFs is wet spinning using spinnerets (also termed needles or tips in some literature). The CNF spinning gel is extruded through the narrow channels and is deformed to be shaped into continuous flow like fibers before it reaches the coagulation bath (Fig. 4a). At the nano-scale, CNFs are oriented and assembled into flowing gels. Apparently, at a given spinning rate, the length of the spinnerets determines the time that fibrils are under shearing, which provides controllable shear thinning and orienting effects on the spinning suspensions. Moreover, the inner diameter of the spinnerets also influences the shear in terms of flow profiles which will be discussed in detail later.

Microfluidic spinning using the flow focusing method is another type of spinning scheme (Fig. 6). In this set-up, a flow-focusing device containing coaxial channels is usually used, where the flows in the sheath channels help generate accelerating flows to align CNFs in the core flow, and induce gelation to lock their alignment simultaneously.[67] Note that the first sheath flow with pH larger than the pK_a of the anionic groups on nanocelluloses promotes alignment, while the second sheath flow with pH lower than pK_a induces protonation and coagulation (Fig. 6b). Different from the spinneret set-up where CNF suspensions should be in a semi-dilute or concentrated regime (normally $G' \geq G''$), microfluidic spinning requires the CNF suspensions in the first half of the semi-dilute or dilute regime ($G' < G''$) to achieve intense deformation.[71] Note that suspensions at very high concentrations with gel-like properties will be torn into fragments.[71] The feasibility of using flowing state suspensions may be attributed to the fact that the second sheath flow consisting of gel-initiators (usually acids) can quickly coagulate fibrils in the spinning flow while they are still under extensional flow field, ensuring there is enough fibril connectivity in fibers when they exit microfluidic channels.

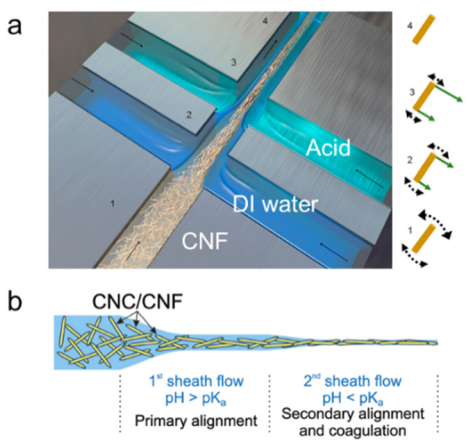

Fig. 6 (a) Schematic of a typical flow-focusing device with double channels used for CNF assembly.[67] (b) The schematic presentation of nanocellulose orientation and gelation in the microfluidic device.[71] Adapted with permission from ref. 71. Copyright 2019 Wiley.

Spinning rate

To control the CNF assembly and modify fiber properties, one key factor is the different applied forces/pressures through the spinneret to give different shearing effects. A high rate is expected to deform the CNF network and align CNFs through the spinning flow more easily.[55] As discussed before, CNF suspensions at shear thinning fit the Ostwald-de Waele power law (eqn (1)). Assuming the spinneret is a circular pipe and the spinning flow is in the laminar state, the correlation between the shear rate ($\dot{\gamma}_w$) and the shear stress (τ_w) applied at the spinneret wall can be expressed as follows:

$$\dot{\gamma}_w = \left(\frac{\tau_w}{K}\right)^{\frac{1}{n}} \quad (2)$$

And the correlation between the shear rate applied at the wall and the spinning rate can be expressed as follows:

$$\dot{\gamma}_w = \frac{3n+1}{n}\frac{Q}{\Pi R^3} = \left(\frac{3n+1}{4n}\right)\frac{8v}{D} \quad (3)$$

where Q is the volumetric spinning rate, v is the spinning velocity, R and D are the radius and diameter of the spinneret, respectively. From the equations above, it is known that shear stress is a function of shear rate and suspension viscosity, and shear rate is a function of spinning rate and capillary radius.[42,87] Therefore, increasing the spinning rate or reducing the spinneret diameter is expected to increase the shear stress exerted on the spinning suspensions.

An increasing spinning rate has been demonstrated as a universal route to promote nanocellulose alignment[59,63,84,88,89] and thus increase the modulus and strength of fibers.[59,63,84,87–89] However, when the spinning rate is increased over a certain threshold, the tensile strength of fibers is reported to reach a plateau level.[59] For instance, too high spinning rates (from 17 to 23 m min^{-1}) generate inferior mechanical properties (modulus from 18.7 to 16.7 GPa).[87] Although the exact orientation indices are not provided, one possible reason is that the CNF spinning flow may change from a laminar flow to a turbulent flow at a high speed, causing lower CNF orientation and defect in the final fibers.[55,56]

Other than increasing the extruding forces/pressures, which may be limited by the equipment, reducing the spinneret diameter is another way to increase the shear rate. However, so far only one study has attempted to do so in which the spinneret diameter decreased from 960 to 380 μm and the Young's

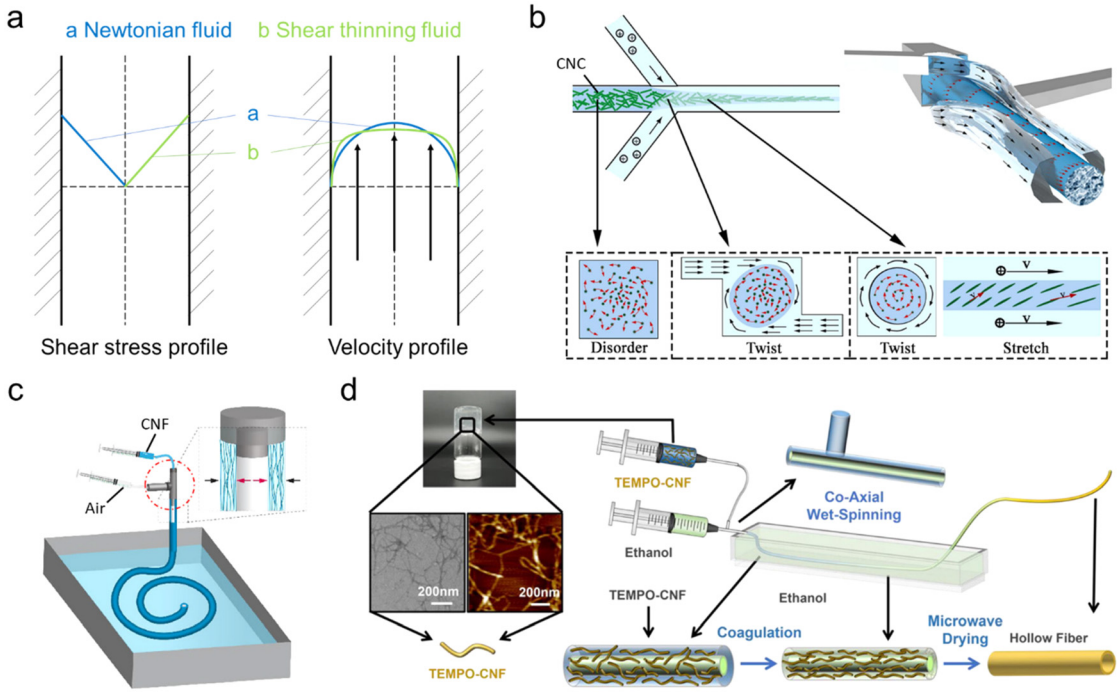

Fig. 7 (a) Estimated shear stress profile and velocity profile within the spinning spinneret. Schematic presentation of special wet spinning spinnerets: (b) convection focusing device.[70] Adapted with permission from ref. 70. Copyright 2018 Elsevier. (c) Coaxial spinning device with compressed air as the inner flow.[91] (d) Coaxial spinning device with coagulation batch as the inner flow.[125] Adapted with permission from ref. 125. Copyright 2023 ACS.

modulus only increased by ~10% (from 21.4 GPa to 24.3 GPa).[87] The reason has been already discussed that might be the turbulent flow at very high spinning rates. This indicates smaller spinneret diameter cannot amplify the orientation effect in certain set-ups.

One curious finding is that the improved CNF orientation by regulating spinning rates doesn't compromise fiber extensibility (aka strain at break) in most studies,[59,63,87,89] though one study has reported a controversial result.[88] Two hypothesizes can be proposed: (1) orientation is induced before coagulation when nanocellulose is free-flowing, while after coagulation, poorly connected regions may form and act as structural defects to promote sliding; (2) non-crystalline regions or residual hemicellulose of CNFs is the main plasticizer governing the deformation.

Challenges and opportunities

One thing that has been normally ignored in most CNF wet-spun fiber studies is that the shear stress along the spinneret radius is not evenly distributed in the spinneret, and the spinning flow has a gradient of velocity along the radius. The shear stress is in linear correlation with the radius, and its velocity profile can be visualized in Fig. 7a, demonstrating the differences between Newtonian and shear thinning fluids. Shear stress at the spinneret wall is the strongest, while it gradually decreases to zero approaching the radius center. Note that once the shear stress is lower than the yield stress of the fibril network (CNF suspension), then it cannot break and disentangle the CNF network and only cause fibril flocculation other than tangential alignment.[42] As a result, CNFs in the final wet-spun fiber are not completely in the best orientated configuration, especially those near the center. Summarizing the literature data, the upper limit of the orientation index for the wet-spun fibers without drawing is under 0.80 (~0.79),[42,53,59,86,88–90] while fibers spun by microfluidic spinning can easily surpass 0.80.[67]

One unique feature of the wet spinning process is that the cross-sectional structure can be tailored by altering the morphologies of spinnerets. For example, hollow-structured fibers can be produced *via* coaxial spinneret set-ups, while the core flow can be either compressed air (Fig. 7c) or the coagulation bath (Fig. 7d) to hold the shell CNF flow. Moreover, fibers with a torsional structure are achieved in a self-twist microfluidic chip with a staggered channel structure, guiding the fibrils to undergo a twist flow (Fig. 7b). These results highlight the prospects and potentials of advanced system design *via* wet spinning for utilizing nanocellulose as building blocks towards advanced structural and functional materials.

Coagulation process

The coagulation process refers to the solvent or/and solute exchange between the freshly extruded fibers and the surrounding media, in order to enable solidification of the fibers with certain shapes, as well as sufficient wet-strength so that they can be lifted and transferred to the next processing stage.

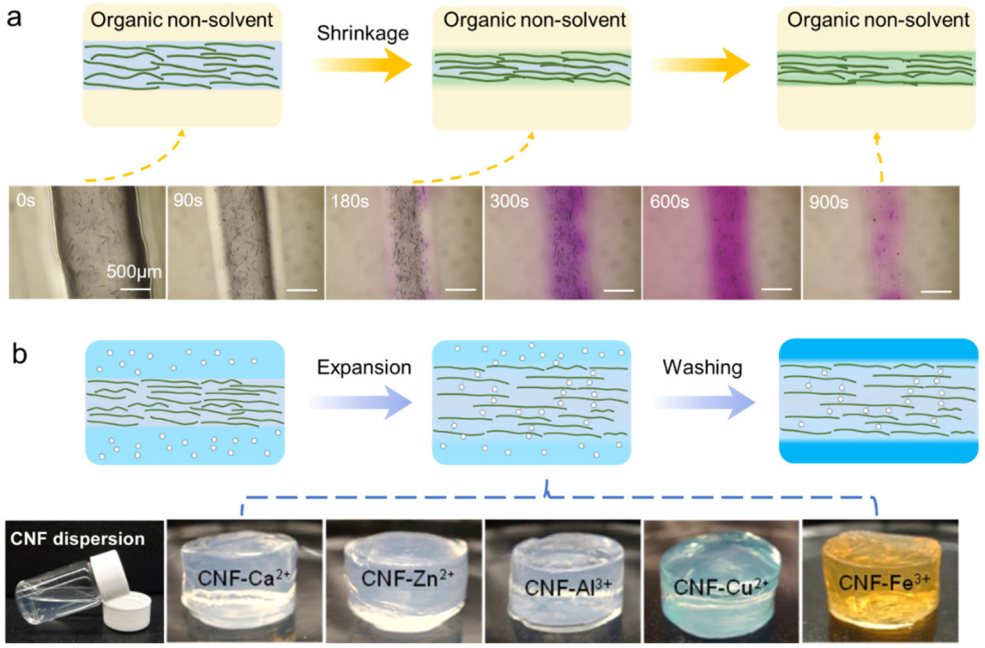

Fig. 8 Schematic presentations of the coagulation process using different coagulation baths and the corresponding still-wet fibers: (a) organic non-solvents.[51] Adapted with permission from ref. 51. Copyright 2023 Elsevier. (b) Ion solutions containing acids or salts.[126] Adapted with permission from ref. 126. Copyright 2013 ACS.

From the nano-structural perspective, nanofibrils are forming a more rigid network. Note that the high orientation of nanocelluloses induced by the high-shear extruding process should be preserved as much as possible, to ensure favorable mechanical properties along the fiber length axis. Currently, there are two types of coagulation baths: organic non-solvents such as acetone[59,63] and ethanol;[51,90] ionic solutions containing either acids (*e.g.* HCl)[91,92] or salts (*e.g.* $CaCl_2$).[87,88]

Organic non-solvents as the coagulation bath

The diffusion between the water within the extruded fiber and the surrounding coagulant is critical, since it will affect the internal structure and subsequent properties of the final fibers. Upon coagulation, water will diffuse out to cause fiber shrinkage, which also promotes the formation of a more compact CNF network. This leads to the formation of fiber shapes and increased wet-strength, allowing them to be lifted and transferred to the next processing step, *i.e.* drying (Fig. 8a). Thus, a suitable organic non-solvent needs to have the following properties: (1) miscible with water to promote efficient dehydration and shrinkage of the fiber, (2) moderate polarity and the ability to promote interaction between fibrils,[93] and (3) low surface tension so that it won't demolish the fibril network during the drying processes afterward. So far, acetone and ethanol have been mostly used, while isopropanol[93,94] and tetrahydrofuran[53,93] have also been reported.

Although extremely important, it is challenging to investigate the coagulation process since it is hard to track the dynamic structural changes without disturbing the solvent exchange process. Mao *et al.*[51] have made efforts to observe the solvent exchange process in detail using optical microscopy. TEMPO-CNF suspensions are colored with Nile red, which can be preferably dissolved in ethanol rather than water and display a blue-purple-pink color change in an ethanol/water mixture with an increasing ethanol ratio. Interestingly, the coagulation can be divided into two stages: (1) the shrinking stage in which water comes out from the fiber internals; (2) the solvent exchange stage in which ethanol diffuses inside fibers to replace water. This agrees well with the theory that the intra- and inter-polymer interactions are initially suppressed and then recovered when the exchange happens from a good solvent replaced subsequently by a poor one,[95] resulting in cross-linking to form a rigid network structure.

Regarding the coagulation rate, it apparently depends on the solvent exchange rate, which can be quantified using parameter T:[96]

$$T = \frac{D_{in}}{D_{out}{}^2} \quad (4)$$

where D_{in} is the diffusion coefficient of the coagulant into water (into the fibers) and D_{out} is the diffusion coefficient of water into the coagulant (out of the fibers). As a quick demonstration, T for acetone bath is faster compared to that for ethanol (5580 to 54 630 s cm^{-2}),[96] which is consistent with experimental results, in which acetone can lock the fibril orientation in a faster manner compared to ethanol.[90]

Ionic solvents as the coagulation bath

Different from using organic non-solvents which intend to promote the dehydration of extruded CNF fibers, the use of ionic solvents is to facilitate strong gelation for solidification (Fig. 8b).[74,97] This often relies on the use of highly charged CNFs particularly TEMPO-CNFs or carboxymethylated CNFs in the sodium form (Na form), so that the interfibrillar interaction can be altered by either moderating the surface charge or introducing crosslinks.

The use of acids such as HCl can protonate the carboxyl groups of CNFs, so that the electrostatic repulsion between neighboring CNFs is greatly reduced leading to aggregation and gelation.[90] In comparison, the use of Ca^{2+} or other types of polyvalent metal ions has two functions: (1) screen the surface charge to lower the electrostatic repulsion and (2) diffuse and replace Na^+ to introduce $–COO^––Ca^{2+}–^–OOC–$ crosslinks.[90] This leads to a more rigid CNF network, as well as gelation in a macroscopic view.[66,74] Other than using polyvalent metal ions, Na^+ can also be used, yet the resultant gel-fibers tend to have inferior wet-strength which is hard to handle.[90] Note that the mass transfer rate of water (from inside to outside) is lower than that of the coagulant (H^+ and Ca^{2+} solutions, from outside to inside), thus the fibers swell after coagulation.[90]

The choice of different acids will affect the final CNF fiber properties.[66] Anions with high hydration capacity, such as $H_2PO_4^–$, cannot efficiently diffuse into fibers. This slows the coagulation process and gives inferior wet-strength. Moreover, anions with larger sizes may also disrupt the fibril repacking in the later drying and post-stretching processes.

Additionally, in most cases excess acid or salt is used to promote a fast and efficient ion diffusion during coagulation, and a large number of ions will be loosely adsorbed on the fiber surface.[88] Therefore, a subsequent washing step is a must to remove the residual cations, otherwise the salts will precipitate after drying and interfere with the structure of the final fibers.

Closer to an ion diffusion situation yet in a special gel network, higher ion concentrations, higher temperature and lower CNF concentrations lead to faster coagulation rates.[98]

Comparison between these two types of coagulation baths

Based on the previous discussion, the use of organic non-solvents or ionic solutions follows totally different coagulation mechanisms. This also leads to differences in the final fibers including the cross-section shape and mechanical properties.

Regarding the size/shape after the coagulation, it has been reported that organic solvent tends to give irregular cross-section shapes compared to ionic solution.[90] The hypothesis is that the surrounding non-solvents (ethanol and acetone) diffuse slower than the mass transfer in water, and a rigid surface layer (compact CNF network structure) is formed on the fiber, with a relatively soft core.[90,93] The rigid surface layer is not strong enough to hold the shape when the fiber is settled on the bottom surface of coagulating containers, and the fiber collapses to a thinner shape under gravity.

The impact of the coagulation bath on the mechanical properties of the fiber is significant. It has been reported that fibers coagulated in an ionic solution have higher tensile strength compared to ones in organic non-solvents (315 ± 31.7 MPa in $CaCl_2$, 319 ± 15.2 MPa in HCl and 198 ± 13.8 MPa in acetone) and Young's modulus (18.6 ± 3.7 GPa in $CaCl_2$, 17.0 ± 2.1 GPa in HCl and 16.9 ± 1.4 GPa in acetone).[90] This is attributed to the enhanced interfibrillar interactions and promoted hydrogen bonding when using acid and newly formed crosslinks when using Ca^{2+}.

Drying process

After the coagulation process, the still-wet fibers contain a fair amount of solvent which needs to be dried in a favorable manner to guarantee the fully compact CNF network structure – preferably with minimal porosity while maintaining the high CNF orientation. For the case of using organic solvent as coagulation baths, it is critical to not achieve a 100% solvent exchange, since the evaporation of water can facilitate sufficient shrinkage due to the high surface tension. Moreover, the organic solvent will evaporate rapidly, which leads to the rest drying process dealing with residual water. As for the case of using ionic solvents as coagulation baths, it only needs to remove water.

Different drying methods have been explored, and can be divided into contact drying and non-contact drying (Fig. 3). The former is often achieved using a heating roller, while the latter can be done using hot air, infrared lamps, ovens or microwaves, as well as a simple procedure in which the fibers are just hanged in open air at room temperature. With the goal of making fibers with regular shapes (preferably the original round shape at cross-section), heating rollers will alter the shapes drastically.[61] Room temperature drying may achieve uniform drying, yet the long drying time is a critical disadvantage in actual practice. In comparison, drying at elevated temperatures using hot air, infrared lamps, ovens or microwaves could introduce the horrification effect (co-crystallization of neighboring CNFs), leading to increased modulus for the final fibers. However, it is hard to achieve uniform drying from all angles using hot air and infrared lamps, while oven and microwave drying are often carried out in a closed system which cannot be integrated into continuous production.

Although drying gel-like fibers is a classical and easy process when glancing at, there is still plenty of room for research. For example, higher heat transfer rates can shorten the drying time, but whether it will cause unwanted non-uniform drying regions or even CNF degradation needs further investigation.

Stretching process

Achieving alignment at a higher speed is challenging for nanofibers with a high aspect ratio and concentration due to per-

sistent colloidal entanglement,[63] thus necessitating the introduction of the stretching process.

In conventional synthetic fibers, a post-stretching process is often induced while the polymer is still in the melting state, in order to improve the polymer chain orientation and get rid of some internal defects. For CNF wet-spun fibers, such an objective is also preferred, but the stretching process needs to be done while the fiber is under still-wet conditions. Thus, stretching can be applied at different stages during the wet spinning process – namely pre-drying, in-process drying and post-drying stretching (Fig. 9b). Pre-drying is located between the coagulation and the drying process, the in-process drying is typically located upstream of the end collection roller, involving the implementation of stretching techniques throughout the drying procedure, and the post-drying involves rehydration of fibers using water or steam followed by subsequent stretching.

Notably, the wet-strength of the fibers in the former two situations is not that strong, so stretching in those two steps cannot be too high, otherwise it will introduce defects or even cause breakage of the entire fibers. To deal with this, Zhao *et al.* developed a two-stage stretching system, in which it is firstly stretched 30% and then 10%, resulting in enhanced CNF orientation with fewer nanoscale defects compared to a single stage stretching.[62] Moreover, even if the CNF orientation is introduced, it may not be maintained before the fiber is transferred to the drying process to fully lock it. This has been reported by Kim *et al.*[99] that the CNF orientation created during the pre-drying stretching step will decline significantly during the washing step, making the pre-drying stretching not preferred or even useless.

Post-drying stretching has been the first choice to achieve optimal CNF orientation, thereby enhancing the mechanical properties of the fibers. Mao *et al.*[51] reported a post-stretching (PS) at 25% will increase the mechanical properties by 120% (567 MPa compared to 257 MPa), while no improvement can be seen when using in-process drying. Regarding the stretching ratio, fibers achieved through continuous wet spinning using an organic non-solvent or acid coagulation bath is limited to 40%,[61–63,100] while in a discontinuous wet spinning process with ion crosslinking treatment, the stretching ratio can reach 50–100%.[101]

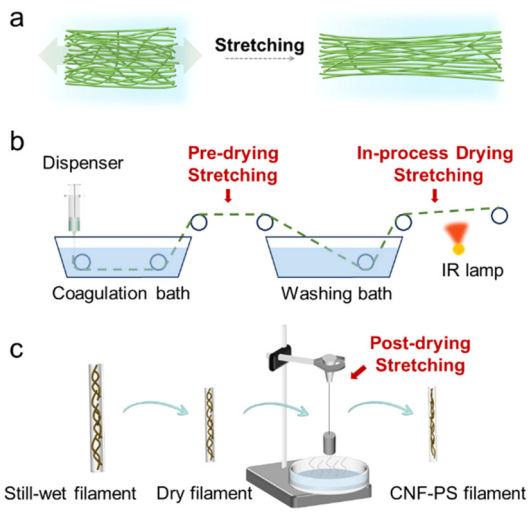

Fig. 9 Schematic presentation of (a) CNF network changes practically the CNF orientation during the wet stretching process, (b) pre-drying and in-process stretching processes and the (c) post-drying stretching process.[51] Adapted with permission from ref. 51. Copyright 2023 Elsevier.

Mechanical properties of CNF wet-spun fibers

By developing or optimizing all the processes above, the mechanical properties of the final CNF wet-spun fibers are one of the most desired objectives. The majority of the reported literature indicates that the tensile strength of wet-spun CNFs from spinnerets and syringes is predominantly concentrated within the range of 200–650 MPa, while Young's modulus is primarily found in the range of 0–40 GPa, as illustrated in Fig. 10b. Clearly post-treatments including stretching can improve the mechanical performance, and a special discontinuous production route may give better results as well. For example, the best mechanical properties obtained in continuous wet spinning (the two-stage stretching process) can have tensile strength and Young's modulus values of 659.8 MPa and 33.2 GPa, respectively,[62] while such properties reach 972 MPa and 84 GPa for a special discontinuous wet spinning process involving a combination of dopamine doping, ion crosslinking and wet stretching.[101] Note that the fibers partially spun by microfluidic devices exhibit significantly enhanced mechanical properties (with Young's modulus of up to 50–85 GPa and tensile strength of up to 1000–1400 MPa) due to their superior orientation and denser assembling structure (Fig. 10a), thanks to the flow-focusing system.

Regarding the objective to replace synthetic fibers,[109–111] natural fibers[22,112–114] or regenerated cellulosic fibers[22,23] in certain applications, the specific strength and modulus are plotted in Fig. 10c. Promisingly, CNFs do have competitive performance, especially in the Young's modulus. Note that the maximum strength values are comparable to its source, wood fibers, indicating a good assembling structure by the wet spinning process. More importantly, its continuous feature can overcome the length limitation of plant fibers, which is a huge advantage in many applications. The last thing we want to comment on is that, although CNF wet-spun fibers can utilize the mechanical properties of CNFs themselves to a large extent, there is still room for improvement, since a single CNF can have strength and Modulus of 2–6 GPa and 130 GPa.[13,15]

Industrial production perspective

Based on the previous discussion, CNFs made through the wet spinning process have superior mechanical properties and sustainable features, indicating great development potential in

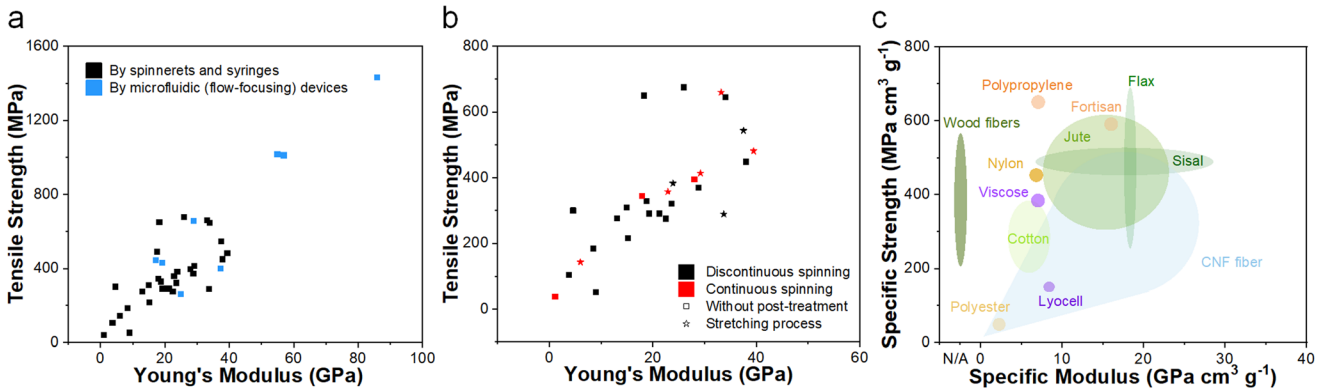

Fig. 10 (a) Ashby plot of tensile strength *versus* Young's modulus for nanocellulose-based fibers spun by spinnerets and syringes, as well as microfluidic devices (flow-focusing method).[52,53,56,59–67,70,71,77,84,86–94,96,99,100,102–108,127,128] (b) Ashby plot of tensile strength *versus* Young's modulus for nanocellulose-based fibers spun from spinnerets and syringes with different spinning processes or treatments.[52,53,56,59–64,77,84,86–91,93,94,96,99,100,102,103,105–108] (c) Overview of specific ultimate strength *versus* specific Young's modulus for a range of synthetic (yellow),[109–111] natural (green)[22,112–114] and regenerated cellulosic (purple)[22,23] fibers/filaments.

high performance applications. Compared to regenerated cellulosic or other polymeric fibers prepared using a well-established wet spinning process, the continuous fabrication of CNF wet-spun fibers remains in an early stage of development, despite the extensive research on process parameters such as spinning suspension, extrusion, coagulation and drying processes on the laboratory scale.

As discussed before, the fundamental configuration of the current continuous wet spinning device typically consists of an extrusion pump, a coagulation bath, a washing bath, several bobbin winders and drying devices (Fig. 11a). Upon reviewing the literature on CNF wet-spun fibers, it is evident that continuous spinning has exhibited superior production efficiency compared to discontinuous spinning, achieving a remarkable production rate of 4–33 m min^{-1}.[61,96,100] However, there is still a considerable gap when compared to viscose yarn's production rate of 500 m min^{-1}.[115] Diverse techniques such as post-stretching,[62,63,99] post-coating,[58] ion exchange,[63] and alternating current (AC) electric field[105] have been implemented to ensure production continuity (Fig. 11a and b). However, despite these commendable efforts, the mechanical properties of terminal fibers remain suboptimal compared to discontinuous spinning. The biggest challenge is to improve the production rate, while guaranteeing the stability, consistency, and reliability of the final fibers. Moreover, the high production rate translates into high spinning rates, which in turn can promote efficient longitudinal axial alignment of CNFs.[61–63] And yes, this undoubtedly necessitates the corresponding matching requirements for each subsequent section, encompassing a sufficient supply of continuous and robust spinning suspension, rapid and stable coagulation, as well as optimal drying conditions.

Spinning suspension

The concentration of the spinning suspension plays a crucial role in ensuring spinnability and continuity, as it directly determines the ultimate fiber qualities. A CNF concentration of 2 wt% and above is typically selected during the continuous spinning process, yet it has not been systematically optimized since it was first reported by Kim *et al.*[99] As the beginning of the wet spinning process, undoubtedly prioritizing the optimization of spinning suspension can open up more avenues for exploring the whole wet spinning process.

The first challenge is to have CNF spinning suspensions at a stable quality level, since it is well known that CNFs can be obtained from different sources, pretreatments and nanofibrillation processes, which provide different chemical compositions, aspect ratios, surface charges, *etc.*[31–33] Actually, this is a common issue for the CNF production industry. In reality, differences in CNFs from batch to batch will drive up the difficulty of adjusting the wet spinning parameters, which can be time consuming and financially unfavorable.

Secondly, as reported by many studies, the CNF concentration needs to be above 1 wt% or even 2 wt%, and a re-concentration process is always needed.[58,61–63,105] Note that most of those studies are using a normal type of homogenization facility which can only produce CNFs with a concentration <1 wt%. Such a reconcentration process is always carried out through centrifugation,[58,61–63,105] vacuum evaporation (often with rotary facility)[31,116] or (ultra-)filtration.[117] The first two are time-consuming and energy-intensive; while the last one cannot be performed in conventional filtering machines because: (1) CNF suspensions at high concentrations are very viscous and require extremely high driving pressure, and (2) CNFs with a thin width/diameter can either pass through the filter (with a big mesh size) too easily or block the filter (with a small mesh size) to significantly reduce the flux. Moreover, the re-concentration process may cause unwanted aggregation. Therefore, while aiming for a sufficient concentration for continuous spinning, it is essential to strike a balance between the drawbacks to achieve optimal preparation efficiency and economic benefits.

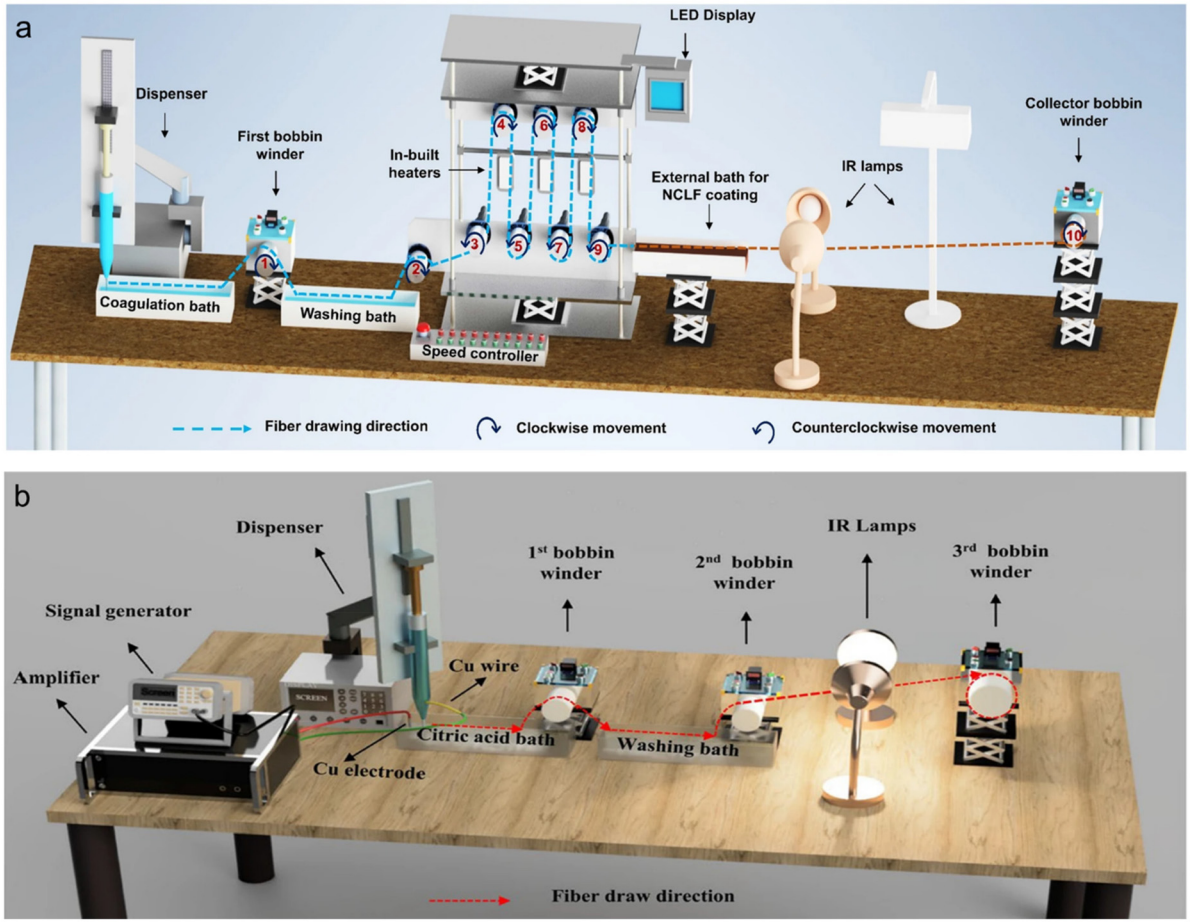

Fig. 11 The representative schematic diagrams of the integrated wet spinning device for the continuous fabrication of CNF wet-spun fibers with (a) in-built heaters[61] and (b) AC electric field.[105] Adapted with permission from ref. 61 and 105. Copyright 2022, 2023 Springer Nature.

Additionally, when the concentration of the spinning suspension reaches a certain level, gases introduced during the stirring or preparation process may become trapped in the high-viscosity spinning suspension, forming bubbles. These bubbles can lead to fiber breakage during the spinning process, making degassing an essential consideration. So far, centrifugation,[58,61,105,118] planetary centrifugal mixer,[91,119] and vacuum oscillation[41,71,120] have been reported. However, the limited degassing capacity and prolonged processing time per cycle pose a bottleneck issue in industrial scale-up. Therefore, developing a large-scale and efficient degassing method is highly desired.

Coagulation process

As discussed before, organic non-solvents and ionic solutions are the two most used types of coagulation baths. For the former one, solvent volatilization is an inevitable issue that may result in safety and cost concerns, especially when using ethanol or acetone. Furthermore, during continuous spinning processes, the diffusion of water within the fibers leads to dilution of the coagulant, thereby imposing higher demands on the circulating supplement section. For the latter one, an additional washing step is a must to remove the excess acids or salts, and the prolonged procedure may also introduce fiber defects. Additionally, the concentration of ions also gradually decreases with increasing running time which also needs a circulating supplement section.

Another challenge is the long coagulation time, up to tens of minutes.[62,90,96] Therefore, in order to ensure continuous spinning, elongating the length of the coagulation tank is necessary. Assuming that the wet spinning rate of CNFs matches that of viscose (500 m min^{-1}), using a coagulation time of 20 s (note that most studies didn't report this value), the length of the coagulation tank needs to be longer than 150 m. This becomes a large construction and the corresponding transmission continuity between adjacent sections needs to be specially designed to maintain the high spinning velocity while dealing with excessive friction and gravity effect. The introduction of conveyor belts[96] was used to address this issue, providing additional support and preventing fiber breakage when hanging in midair, as well as facilitating the winding process. However, it is important to note that an appropriately extended coagulation time is still required to safeguard the fiber's round stiffness and protect it from excessive flattening or collapsing when in contact with the conveyor belt.

Drying process

The drying process is also a critical section in determining the production rate of continuous spinning, however, it is often overlooked in most literature. The ideal case will be drying the fibers homogeneously and efficiently in a fast manner. Traditionally, using external heating sources can do the job, however, CNFs exhibit inferior thermal stability and typically undergo thermal degradation at 230 °C especially with surface carboxyl groups.[121] Also, there are challenges with the heating methods: (1) contact drying using heating rollers will change the cross-section shape; (2) non-contact drying such as infrared light at too high intensity, cannot work on volatile or even combustible solvents like ethanol.

Equipment optimization

The selection and arrangement of equipment are crucial factors in optimizing the system. Nechyporchuk *et al.*[108] employed bobbin winders with a thickness of 5 mm attached to the surface and alternating each 50 mm, enabling drying of the fibers in air without direct contact with the winder surface and preserving their equiaxed cross-sections. Kim *et al.*,[99] on the other hand, adjusted the height of the collection bobbin winders to optimize winder usage and minimize the contact area between the fibers and winders. Additionally, the angle between the collection bobbin winder and the penultimate bobbin winder is optimized to be acute in order to achieve an ideal position, thereby ensuring efficient fiber drying.[61]

Quick remark

If we make production capacity, *i.e.* the spinning rate as the main objective, all the manufacturing sections within the wet spinning process need to coordinate with each other to be optimized. The starting spinning dispersion needs to have the right spinnability, the spinning process needs to be able to orient the CNFs while maintaining a continuous flow, the coagulation needs to be fast and give sufficient wet-strength, and the drying process needs to be efficient. More importantly, the optimization of continuous wet spinning equipment involves strategically arranging the coagulation bath, washing bath, bobbin winders, and drying devices, as well as taking into account the economic, safety and environmental aspects.

Conclusions

In the light of engineering strong man-made cellulosic fibers by reconstructing plant fibers, wet spinning of cellulose nanofibrils (CNFs) into continuous fibers offers great opportunities and has broad prospects. To optimize the performance of wet-spun CNF fibers, a comprehensive understanding and control of each wet spinning section is needed, which correlates with the changes in both macro and micro perspectives: (1) the bulk material phase changes from viscous gels to dried fibers and (2) the CNF assembling network changes from a dilute and isotropic form to a densely packed and oriented confirmation.

Starting with the CNF spinning suspension preparation, key factors including concentration, aspect ratio, surface charge, processing history, and chemical composition intricately influence the rheological behaviour. The careful balance between the deformation ability and connectivity of CNFs is essential to optimize the spinnability. Moving to the spinning section, both the spinning rate and spinneret design are critical, as they control the extruding flow profile to provide sufficient shearing for CNF orientation, which unfortunately has been simply treated as plug flow in the literature. In the following coagulation process, organic non-solvents promote fiber shrinkage and the formation of a compact CNF network, while ionic solvents induce gelation through electrostatic interactions and cross-linking. As the first and critical step to solidify the extruding fibers into certain shapes with mechanical wet strength, more in-depth studies are urgently needed on this special mass-transfer process crossing the gel state. The drying process aims to lock the oriented CNF networks, while minimizing the generation of defects such as local CNF aggregations and air gaps. Finally, post-drying stretching emerges as the preferred choice for enhancing CNF orientation and fiber mechanical properties.

Besides the need for improving the production capacity (spinning rate) for industrial realization, challenges persist in a holistic optimization approach for spinning suspension stability and continuity, coagulation efficiency, drying methods, along with the need for equipment adjustment and development, in order to promote the CNF wet-spun fibers for high-performance applications when compared to synthetic fibers.

In essence, this review not only elucidates the intricacies of the wet spinning process, but also emphasizes the structure–property relationships between the CNFs and the final wet-spun fibers. By utilizing the plant fibers' own building blocks, we stand at the forefront of a promising era in fiber science from nanostructures to industrial applications, representing a significant stride towards sustainable and innovative practices in the world of fiber materials.

Conflicts of interest

The authors declare no competing financial interest.

Acknowledgements

We acknowledge the funding from the National Natural Science Foundation of China (Grants No. 22108244 and 22278359), the "Pioneer" and "Leading Goose" R&D Program of Zhejiang (Grant No. 2022C01234), and the Quzhou Science and Technology Project (Grant No. 2022Z09). We thank Da Zhang, Roufen Wu, Jiahe Li, Ting Jin, Chengxi Zhang, Kexin Zhou, Yuxuan Xia, and Xiaoting Zhao for useful discussions.

References

1 Grand view research, *Synthetic Fibers Market Size, Share & Trends Report*, 2023.
2 J. E. McIntyre, *Synthetic fibres: nylon, polyester, acrylic, polyolefin*, CRC Press, 2005.
3 D. Feldman and A. Barbalata, *Synthetic polymers: technology, properties, applications*, Chapman & Hall, 1996.
4 S. J. Eichhorn, J. W. S. Hearle, M. Jaffe and T. Kikutani, *Handbook of textile fibre structure: Fundamentals and manufactured polymer fibres*, Woodhead Publishing, 2009, vol. 1.
5 X. Yang, L. A. Berglund, X. Yang and A. Berglund, *Adv. Mater.*, 2021, **33**, 2001118.
6 C. Chen, Y. Kuang, S. Zhu, I. Burgert, T. Keplinger, A. Gong, T. Li, L. Berglund, S. J. Eichhorn and L. Hu, *Nat. Rev. Mater.*, 2020, **5**, 642–666.
7 Z. Su, Y. Yang, Q. Huang, R. Chen, W. Ge, Z. Fang, F. Huang and X. Wang, *Prog. Mater. Sci.*, 2022, **125**, 100917.
8 H. Nawaz, X. Zhang, S. Chen, T. You and F. Xu, *Carbohydr. Polym.*, 2021, **267**, 118135.
9 S. Tao, C. Zhang, Y. Chen, S. Qin and H. Qi, *Carbohydr. Polym.*, 2022, **283**, 119151.
10 D. Wang, Y. Gu, S. Feng, W. Yang, H. Dai, H. Xiao and J. Han, *Green Chem.*, 2023, **25**, 9020–9044.
11 Y. Nishiyama, P. Langan and H. Chanzy, *J. Am. Chem. Soc.*, 2002, **124**, 9074–9082.
12 N. G. Taylor, *New Phytol.*, 2008, **178**, 239–252.
13 I. Sakurada, Y. Nukushina and T. Ito, *J. Polym. Sci.*, 1962, **57**, 651–660.
14 G. Josefsson, F. Berthold and E. K. Gamstedt, *Int. J. Solids Struct.*, 2014, **51**, 945–953.
15 T. Saito, R. Kuramae, J. Wohlert, L. A. Berglund and A. Isogai, *Biomacromolecules*, 2013, **14**, 248–253.
16 M. S. Smole, S. Hribernik and K. S. Kleinschek, *Advances in Agrophysical Research*, 2013, 369–398.
17 R. Kumar, F. Hu, C. A. Hubbell, A. J. Ragauskas and C. E. Wyman, *Bioresour. Technol.*, 2013, **130**, 372–381.
18 X. Yang and L. A. Berglund, *ACS Sustainable Chem. Eng.*, 2018, **6**, 501–510.
19 C. J. Biermann, *Handbook of Pulping and Papermaking*, Elsevier, 1996.
20 X. Yang, F. Berthold and L. A. Berglund, *Biomacromolecules*, 2018, **19**, 3020–3029.
21 H. Shen, T. Sun and J. Zhou, *Macromol. Mater. Eng.*, 2023, **308**, 2300089.
22 A. K. Bledzki and J. Gassan, *Prog. Polym. Sci.*, 1999, **24**, 221–274.
23 A. Yamamoto, A. J. Uddin, Y. Gotoh, M. Nagura and M. Iwata, *J. Appl. Polym. Sci.*, 2011, **119**, 3152–3161.
24 T. Kim, D. Kim and Y. Park, *J. Cleaner Prod.*, 2022, **376**, 134226.
25 C. Yadav, J. M. Lee, P. Mohanty, X. Li and W. D. Jang, *Nanoscale*, 2023, **15**, 15108–15145.
26 E. Kontturi, P. Laaksonen, M. B. Linder, Nonappa, A. H. Gröschel, O. J. Rojas and O. Ikkala, *Adv. Mater.*, 2018, **30**, 1703779.
27 B. Thomas, M. C. Raj, B. K. Athira, H. M. Rubiyah, J. Joy, A. Moores, G. L. Drisko and C. Sanchez, *Chem. Rev.*, 2018, **118**, 11575–11625.
28 E. J. Foster, R. J. Moon, U. P. Agarwal, M. J. Bortner, J. Bras, S. Camarero-Espinosa, K. J. Chan, M. J. D. Clift, E. D. Cranston, S. J. Eichhorn, D. M. Fox, W. Y. Hamad, L. Heux, B. Jean, M. Korey, W. Nieh, K. J. Ong, M. S. Reid, S. Renneckar, R. Roberts, J. A. Shatkin, J. Simonsen, K. Stinson-Bagby, N. Wanasekara and J. Youngblood, *Chem. Soc. Rev.*, 2018, **47**, 2609–2679.
29 M. Henriksson, G. Henriksson, L. A. Berglund and T. Lindström, *Eur. Polym. J.*, 2007, **43**, 3434–3441.
30 T. Li, C. Chen, A. H. Brozena, J. Y. Zhu, L. Xu, C. Driemeier, J. Dai, O. J. Rojas, A. Isogai, L. Wågberg and L. Hu, *Nature*, 2021, **590**, 47–56.
31 F. Jiang and Y. Lo Hsieh, *Carbohydr. Polym.*, 2013, **95**, 32–40.
32 F. Jiang, T. Li, Y. Li, Y. Zhang, A. Gong, J. Dai, E. Hitz, W. Luo and L. Hu, *Adv. Mater.*, 2018, **30**, 1703453.
33 L. Song, C. Yan, X. Che, S. Yao, S. Nie and H. Xu, *Curr. Nanosci.*, 2022, **19**, 459–472.
34 T. Saito, Y. Nishiyama, J. L. Putaux, M. Vignon and A. Isogai, *Biomacromolecules*, 2006, **7**, 1687–1691.
35 T. Saito, S. Kimura, Y. Nishiyama and A. Isogai, *Biomacromolecules*, 2007, **8**, 2485–2491.
36 N. Mahfoudhi and S. Boufi, *Cellulose-Reinforced Nanofibre Composites: Production, Properties and Applications*, Woodhead Publishing, 2017, pp. 277–304.
37 O. M. Vanderfleet and E. D. Cranston, *Nat. Rev. Mater.*, 2020, **6**, 124–144.
38 Y. Si, Q. Lin, F. Zhou, J. Qing, H. Luo, C. Zhang, J. Zhang and R. Cha, *Carbohydr. Polym.*, 2022, **295**, 119899.
39 W. Hao, M. Wang, F. Zhou, H. Luo, X. Xie, F. Luo and R. Cha, *Carbohydr. Polym.*, 2020, **243**, 116466.
40 T. Rosén, B. S. Hsiao, L. D. Söderberg, T. Rosén, L. D. Söderberg and B. S. Hsiao, *Adv. Mater.*, 2021, **33**, 2001238.
41 O. Nechyporchuk, M. N. Belgacem and F. Pignon, *Biomacromolecules*, 2016, **17**, 2311–2320.
42 M. J. Lundahl, M. Berta, M. Ago, M. Stading and O. J. Rojas, *Eur. Polym. J.*, 2018, **109**, 367–378.
43 B. Nazari, V. Kumar, D. W. Bousfield and M. Toivakka, *J. Rheol.*, 2016, **60**, 1151–1159.
44 N. Quennouz, S. M. Hashmi, H. S. Choi, J. W. Kim and C. O. Osuji, *Soft Matter*, 2015, **12**, 157–164.
45 A. Naderi, T. Lindström and J. Sundström, *Cellulose*, 2014, **21**, 1561–1571.
46 L. Jowkarderis and T. G. M. Van De Ven, *Carbohydr. Polym.*, 2015, **123**, 416–423.
47 D. Tatsumi, S. Ishioka and T. Matsumoto, *Nihon Reoroji Gakkaishi*, 2002, **30**, 27–32.
48 M. J. Solomon and P. T. Spicer, *Soft Matter*, 2010, **6**, 1391–1400.
49 L. Mendoza, W. Batchelor, R. F. Tabor and G. Garnier, *J. Colloid Interface Sci.*, 2018, **509**, 39–46.

50 M. Nordenström, A. Fall, G. Nyström and L. Wågberg, *Langmuir*, 2017, **33**, 9772–9780.
51 H. Mao, P. Niu, Z. Zhang, Y. Kong, W. J. Wang and X. Yang, *Carbohydr. Polym.*, 2023, **313**, 120881.
52 M. J. Lundahl, A. G. Cunha, E. Rojo, A. C. Papageorgiou, L. Rautkari, J. C. Arboleda and O. J. Rojas, *Sci. Rep.*, 2016, **6**, 1–4.
53 J. G. Torres-Rendon, F. H. Schacher, S. Ifuku and A. Walther, *Biomacromolecules*, 2014, **15**, 2709–2717.
54 T. Benselfelt and L. Wågberg, *Biomacromolecules*, 2019, **20**, 2406–2412.
55 M. J. Lundahl, V. Klar, L. Wang, M. Ago and O. J. Rojas, *Ind. Eng. Chem. Res.*, 2017, **56**, 8–19.
56 K. M. O. Håkansson, *Cellulose*, 2021, **28**, 881–895.
57 K. Li, C. M. Clarkson, L. Wang, Y. Liu, M. Lamm, Z. Pang, Y. Zhou, J. Qian, M. Tajvidi, D. J. Gardner, H. Tekinalp, L. Hu, T. Li, A. J. Ragauskas, J. P. Youngblood and S. Ozcan, *ACS Nano*, 2021, **15**, 3646–3673.
58 P. S. Panicker, D. O. Agumba and J. Kim, *ACS Sustainable Chem. Eng.*, 2022, **10**, 10024–10033.
59 S. Iwamoto, A. Isogai and T. Iwata, *Biomacromolecules*, 2011, **12**, 831–836.
60 L. Geng, B. Chen, X. Peng and T. Kuang, *Mater. Des.*, 2017, **136**, 45–53.
61 P. S. Panicker, H. C. Kim and J. Kim, *Sci. Rep.*, 2023, **13**, 13137.
62 X. Zhao, S. Chen, Z. Wu, N. Sheng, M. Zhang, Q. Liang, Z. Han and H. Wang, *Carbohydr. Polym.*, 2022, **282**, 119133.
63 J. Yao, S. Chen, Y. Chen, B. Wang, Q. Pei and H. Wang, *ACS Appl. Mater. Interfaces*, 2017, **9**, 20330–20339.
64 Q. Liang, D. Zhang, P. Ji, N. Sheng, M. Zhang, Z. Wu, S. Chen and H. Wang, *ACS Appl. Mater. Interfaces*, 2021, **13**, 1545–1554.
65 K. M. O. Håkansson, A. B. Fall, F. Lundell, S. Yu, C. Krywka, S. V. Roth, G. Santoro, M. Kvick, L. P. Wittberg, L. Wågberg and L. D. Söderberg, *Nat. Commun.*, 2014, **5**, 4018.
66 N. Mittal, T. Benselfelt, F. Ansari, K. Gordeyeva, S. V. Roth, L. Wågberg and L. D. Söderberg, *Angew. Chem.*, 2019, **131**, 18735–18742.
67 N. Mittal, F. Ansari, V. G. Krishne, C. Brouzet, P. Chen, P. T. Larsson, S. V. Roth, F. Lundell, L. Wågberg, N. A. Kotov and L. D. Söderberg, *ACS Nano*, 2018, **12**, 6378–6388.
68 Z. Xu, J. Zhou, D. Li, G. Zhu and N. Lin, *ACS Sustainable Chem. Eng.*, 2023, **11**, 10895–10905.
69 V. Hynninen, P. Mohammadi, W. Wagermaier, S. Hietala, M. B. Linder, O. Ikkala and Nonappa, *Eur. Polym. J.*, 2019, **112**, 334–345.
70 J. Wang, Q. Gao, Y. Wang, X. Liu and S. Nie, *Ind. Crops Prod.*, 2022, **178**, 114599.
71 O. Nechyporchuk, K. M. O. Håkansson, K. Gowda, V. F. Lundell, B. Hagström and T. Köhnke, *Adv. Mater. Technol.*, 2019, **4**, 1800557.
72 L. Geng, N. Mittal, C. Zhan, F. Ansari, P. R. Sharma, X. Peng, B. S. Hsiao and L. D. Söderberg, *Macromolecules*, 2018, **51**, 1498–1506.
73 H. Fukuzumi, R. Tanaka, T. Saito and A. Isogai, *Cellulose*, 2014, **21**, 1553–1559.
74 A. B. Fall, S. B. Lindström, O. Sundman, L. Ödberg and L. Wågberg, *Langmuir*, 2011, **27**, 11332–11338.
75 L. Geng, A. Naderi, Y. Mao, C. Zhan, P. Sharma, X. Peng and B. S. Hsiao, *ACS Symp. Ser.*, 2017, **1251**, 113–132.
76 T. Benselfelt, M. Nordenström, M. M. Hamedi and L. Wågberg, *Nanoscale*, 2019, **11**, 3514–3520.
77 B. Pingrey and Y. Lo Hsieh, *Biomacromolecules*, 2022, **23**, 1269–1277.
78 J. A. Sirviö, M. Visanko and H. Liimatainen, *Green Chem.*, 2015, **17**, 3401–3406.
79 D. Klemm, E. D. Cranston, D. Fischer, M. Gama, S. A. Kedzior, D. Kralisch, F. Kramer, T. Kondo, T. Lindström, S. Nietzsche, K. Petzold-Welcke and F. Rauchfuß, *Mater. Today*, 2018, **21**, 720–748.
80 T. Benselfelt, N. Kummer, M. Nordenström, A. B. Fall, G. Nyström and L. Wågberg, *ChemSusChem*, 2023, **16**, e202201955.
81 X. Yang, M. S. Reid, P. Olsén and L. A. Berglund, *ACS Nano*, 2020, **14**, 724–735.
82 M. Oprea and D. M. Panaitescu, *Molecules*, 2020, **25**, 4045.
83 C.-W. W. Park, S.-Y. Y. Han, S.-K. K. Choi and S.-H. H. Lee, *BioResources*, 2017, **12**, 6298–6308.
84 C. W. Park, J. S. Park, S. Y. Han, E. A. Lee, G. J. Kwon, Y. H. Seo, J. G. Gwon, S. Y. S. H. Lee and S. Y. S. H. Lee, *Polymers*, 2020, **12**, 949.
85 K. Jin, D. Zhang, B. Pan, K. H. Lim, T. Abitbol, W. J. Wang and X. Yang, *Chem. Eng. J.*, 2023, **473**, 145189.
86 L. Wang, M. Borghei, A. Ishfaq, P. Lahtinen, M. Ago, A. C. Papageorgiou, M. J. Lundahl, L. S. Johansson, T. Kallio and O. J. Rojas, *ACS Sustainable Chem. Eng.*, 2020, **8**, 8549–8561.
87 H. C. Kim, D. Kim, J. Y. Lee, L. Zhai and J. Kim, *Int. J. Precis. Eng. Manuf. – Green Technol.*, 2019, **6**, 567–575.
88 A. Kafy, H. C. Kim, L. Zhai, J. J. W. Kim, L. Van Hai, T. J. Kang and J. J. W. Kim, *Sci. Rep.*, 2017, **7**, 17683.
89 P. Mohammadi, M. S. Toivonen, O. Ikkala, W. Wagermaier and M. B. Linder, *Sci. Rep.*, 2017, **7**, 1–10.
90 L. Wang, M. J. Lundahl, L. G. Greca, A. C. Papageorgiou, M. Borghei and O. J. Rojas, *Sci. Rep.*, 2019, **9**, 1–11.
91 G. Reyes, R. Ajdary, M. R. Yazdani and O. J. Rojas, *ACS Appl. Polym. Mater.*, 2022, **4**, 2908–2916.
92 A. Marais, L. Wagberg, J. Erlandsson and L. D. Soderberg, *ACS Appl. Nano Mater.*, 2020, **3**, 10246–10251.
93 A. Walther, J. V. I. Timonen, I. Díez, A. Laukkanen and O. Ikkala, *Adv. Mater.*, 2011, **23**, 2924–2928.
94 H. C. Kim, J. W. Kim, L. Zhai and J. Kim, *Cellulose*, 2019, **26**, 5821–5829.
95 L. Xu, S. Gao, Q. Guo, C. Wang, Y. Qiao and D. Qiu, *Adv. Mater.*, 2020, **32**(52), DOI: **10.1002/adma.202004579**.

96 M. J. Lundahl, V. Klar, R. Ajdary, N. Norberg, M. Ago, A. G. Cunha and O. J. Rojas, *ACS Appl. Mater. Interfaces*, 2018, **10**, 27287–27296.
97 L. Valencia, E. M. Nomena, S. Monti, W. Rosas-Arbelaez, A. P. Mathew, S. Kumar and K. P. Velikov, *Nanoscale*, 2020, **12**, 15652–15662.
98 C.-K. Liu, J. A. Cuculo and B. Smith, *J. Polym. Sci., Part B: Polym. Phys.*, 1990, **28**, 449–465.
99 H. C. Kim, P. Panicker, L. Zhai, Y. Zhu, J. Kim and P. S. Panicker, *Nano-, Bio-, Info-Tech Sensors, 3D Syst. IV. SPIE*, 2020, **11378**, 11–15.
100 A. Tripathi, M. Ago, S. A. Khan and O. J. Rojas, *ACS Appl. Mater. Interfaces*, 2018, **10**, 44776–44786.
101 T. Guo, Z. Wan, Y. Yu, H. Chen, Z. Wang, D. Li, J. Song, O. J. Rojas and Y. Jin, *ACS Appl. Mater. Interfaces*, 2022, **14**, 16809–16819.
102 Q. Gao, J. Wang, J. Liu, Y. Wang, J. Guo, Z. Zhong and X. Liu, *Cellulose*, 2021, **28**, 7995–8008.
103 G. Reyes, M. J. Lundahl, S. Alejandro-Martín, L. E. Arteaga-Pérez, C. Oviedo, A. W. T. King and O. J. Rojas, *Biomacromolecules*, 2020, **21**, 878–891.
104 N. Ren, S. Chen, M. Cui, R. Huang, W. Qi, Z. He and R. Su, *Carbohydr. Polym.*, 2022, **296**, 119945.
105 P. S. Panicker, H. C. Kim, D. O. Agumba, R. M. Muthoka and J. Kim, *Cellulose*, 2022, **29**, 3499–3511.
106 S. Hooshmand, Y. Aitomäki, L. Berglund, A. P. Mathew and K. Oksman, *Compos. Sci. Technol.*, 2017, **150**, 79–86.
107 H. Mertaniemi, C. Escobedo-Lucea, A. Sanz-Garcia, C. Gandía, A. Mäkitie, J. Partanen, O. Ikkala and M. Yliperttula, *Biomaterials*, 2016, **82**, 208–220.
108 O. Nechyporchuk, R. Bordes and T. Köhnke, *ACS Appl. Mater. Interfaces*, 2017, **9**, 39069–39077.
109 J. Guan, D. Porter and F. Vollrath, *Polymer*, 2012, **53**, 2717–2726.
110 M. De Araújo, *Fibrous and Composite Materials for Civil Engineering Applications*, Woodhead Publishing, 2011, pp. 3–28.
111 J. E. Riccieri, L. H. De Carvalho and A. Vázquez, *Polym. Compos.*, 1999, **20**, 29–37.
112 A. Paul and S. Thomas, *J. Appl. Polym. Sci.*, 1997, **63**, 247–266.
113 X. Li, L. G. Tabil and S. Panigrahi, *J. Polym. Environ.*, 2007, **15**, 25–33.
114 W. P. Inacio, F. P. D. Lopes and S. N. Monteiro, *Matéria*, 2010, **15**, 124–130.
115 M. Nywlt, *Chem. Fibers Int.*, 2002, **52**, 170–172.
116 J. Zhou and Y. Lo Hsieh, *Nano Energy*, 2020, **68**, 104305.
117 Q. Wang, Q. Yao, J. Liu, J. Sun, Q. Zhu and H. Chen, *Cellulose*, 2019, **26**, 7585–7617.
118 C. Qiu, K. Zhu, X. Zhou, L. Luo, J. Zeng, R. Huang, A. Lu, X. Liu, F. Chen, L. Zhang and Q. Fu, *ACS Sustainable Chem. Eng.*, 2018, **6**, 4056–4067.
119 L. Wang, M. Ago, M. Borghei, A. Ishaq, A. C. Papageorgiou, M. Lundahl and O. J. Rojas, *ACS Sustainable Chem. Eng.*, 2019, **7**, 6013–6022.
120 Z. Zhang, H. Mao, Y. Kong, P. Niu, J. Zheng, P. Liu, W. J. Wang, Y. Li and X. Yang, *Small*, 2023, 2305924.
121 K. Lichtenstein and N. Lavoine, *Polym. Degrad. Stab.*, 2017, **146**, 53–60.
122 M. C. Iglesias, P. S. McMichael, O. Asafu-Adjaye, B. K. Via and M. S. Peresin, *Cellulose*, 2021, **28**, 7969–7979.
123 J. H. Jordan, M. W. Easson, B. Dien, S. Thompson and B. D. Condon, *Cellulose*, 2019, **26**, 5959–5979.
124 X. Yang, E. Jungstedt, M. S. Reid and L. A. Berglund, *Macromolecules*, 2021, **54**, 4443–4452.
125 P. Niu, H. Mao, K. H. Lim, Q. Wang, W. J. Wang and X. Yang, *ACS Nano*, 2023, **17**, 14686–14694.
126 H. Dong, J. F. Snyder, K. S. Williams and J. W. Andzelm, *Biomacromolecules*, 2013, **14**, 3338–3345.
127 H. G. Wise, H. Takana, F. Ohuchi and A. B. Dichiara, *ACS Appl. Mater. Interfaces*, 2020, **12**, 28568–28575.
128 N. Mittal, R. Jansson, M. Widhe, T. Benselfelt, K. M. O. Håkansson, F. Lundell, M. Hedhammar and L. D. Söderberg, *ACS Nano*, 2017, **11**, 5148–5159.